

Exchange-bias effect in Fe/Cr(211) double superlattice structures

J. S. Jiang, G. P. Felcher, A. Inomata, R. Goyette, C. Nelson, and S. D. Bader

Argonne National Laboratory, Argonne, Illinois 60439

(Received 29 November 1999)

Shifted hysteresis loops characteristic of the exchange-bias effect between a ferromagnet (F) and an anti-ferromagnet (AF) are demonstrated in “double-superlattice” structures. Utilizing the well-established oscillatory interlayer exchange coupling in Fe/Cr, we have constructed $[\text{Fe/Cr}]^{\text{AF}}/\text{Cr}/[\text{Fe/Cr}]^{\text{F}}$ double superlattices where Fe/Cr superlattices with appropriate Cr-spacer thickness represent the F and the AF. The double superlattices are (211)-oriented epitaxial films sputter grown on single-crystal MgO(110) substrates. The AF/F interface is coherent compared to conventional exchange-bias interfaces consisting of dissimilar AF and F phases. Magnetization results show that AF/F exchange coupling affects the nucleation of reverse magnetic domains, and that the magnitude of the exchange-bias field is given directly by the classic formula for collinear spin structures. The collinear spin distribution is confirmed by polarized neutron reflectivity.

The exchange-bias effect is a well-known but still unresolved phenomenon.¹ Discovered in 1956 by Meiklejohn and Bean in Co-CoO particle systems, it refers to the occurrence of a unidirectional magnetic anisotropy that manifests itself in strikingly shifted hysteresis loops for coupled ferromagnet (F)/antiferromagnet (AF) systems cooled through the Néel temperature in the presence of a magnetic field.² However, despite extensive research effort on various AF/F systems,^{3–8} and important technological applications such as magnetoresistive read heads that utilize exchange bias,⁹ a clear understanding of the microscopic origin of the phenomenon has yet to emerge.

Since its discovery exchange biasing has been interpreted as the result of the exchange interaction at AF/F interfaces: the magnitude of the exchange-bias field is given by balancing the gain in Zeeman energy with the energy cost of interfacial exchange when the ferromagnet reverses its magnetization. In the earliest model¹⁰ it was assumed that the F and AF spin structures are rigid, and that the AF/F interface is perfectly flat and uncompensated. However, such an intuitive picture gives estimated exchange-bias fields that are nearly two orders of magnitude larger than what is typically observed experimentally. Two models have been proposed to address this difficulty: the domain wall model of Mauri *et al.*¹¹ in which an AF domain wall parallel to the interface formed during the magnetization reversal of the ferromagnet reduces the interfacial energy, and the random-field model of Malozemoff¹² in which interfacial disorder such as roughness is treated as a random field giving rise to in-plane AF domains and a reduced but statistically nonvanishing interfacial energy for a finite system. Extending the domain wall model of Mauri *et al.*, Koon¹³ was able to account for the exchange-bias effect observed in fully compensated AF/F interfaces with perpendicular (i.e., spin-flop) coupling.¹⁴ However, by solving the full equation of motion during magnetic reversal, Schulthess and Butler¹⁵ showed that spin-flop coupling alone leads to a uniaxial rather than a unidirectional anisotropy. They further argued that domain wall pinning by interfacial defects is necessary to establish exchange bias. The Malozemoff theory was corroborated by Takano *et al.*¹⁶ who showed the relation between exchange bias and net un-

compensated spins for CoO-Permalloy bilayers at the AF/F interfaces. However, experimental observations do not always agree on the effect of interfacial disorder, as both increased⁶ and decreased⁷ exchange bias due to interfacial disorder have been reported.

To our knowledge, to date there has not been an experimental study that can ascertain the interfacial atomic and spin structures in an exchange-bias system. Suitable atomically flat surfaces do not tend to exist for such studies; there is always at least atomic-scale roughness at the AF/F interface. Since the interface is buried and therefore inaccessible to most surface probes, the AF spin structure at the interface is often assumed to be the same as that of the bulk, while in reality there could be a spin rearrangement at the interface.^{5–7} The reduced lateral coherence due to interfacial roughness or random AF domains renders scattering experiments ineffective.¹⁷ In view of these unresolved issues, it is beneficial to construct a system where the exchange-bias effect can be realized and examined in detail with minimal materials-related complexities.

In this paper, we demonstrate the exchange-bias effect in Fe/Cr *double superlattice* structures. The exchange coupling of ferromagnetic transition-metal layers across a nonmagnetic spacer allows for the creation of magnetic structures with desired magnetic configurations.¹⁸ The interlayer-exchange coupling between Fe layers across a Cr spacer is oscillatory, with a “long” period of 18 Å in Cr thickness.¹⁹ Thus, a double superlattice structure with the configuration $[\text{Fe/Cr}]^{\text{AF}}/\text{Cr}/[\text{Fe/Cr}]^{\text{F}}$, where the superscripts denote anti-ferromagnetic and ferromagnetic coupling within the base Fe/Cr superlattices, constitutes an exchange-bias system with the center Cr layer delineating the AF/F interface. The requisite magnetic anisotropy in the AF for exchange bias is represented by a growth-induced uniaxial anisotropy. It has been shown that (211)-oriented Fe/Cr superlattices epitaxially grown on the MgO(110) substrates have a uniaxial, in-plane, surface magnetic anisotropy, with the easy axis along the Fe/Cr[011] direction.²⁰ The AF/F interfacial coupling, i.e., the intersuperlattice coupling, in the double superlattice system is governed by the thickness of the center Cr layer. Since the 18-Å period of the interlayer coupling is relatively

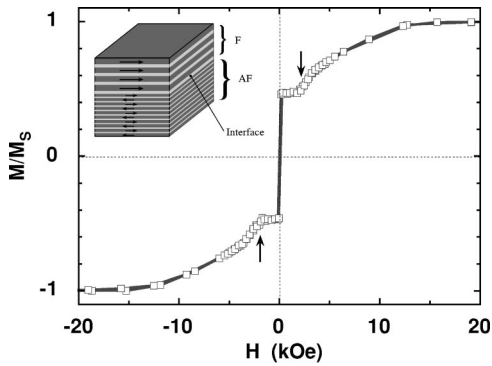


FIG. 1. Room-temperature magnetization curve of an $[\text{Fe}(14 \text{ \AA})/\text{Cr}(11 \text{ \AA})]_{20}/\text{Cr}(9 \text{ \AA})/[\text{Fe}(50 \text{ \AA})/\text{Cr}(20 \text{ \AA})]_5$ double superlattice. The arrows mark spin-flop transitions. Inset: Schematic illustration of a double superlattice structure. The dark layers represent magnetic layers.

long compared to the range of the interatomic exchange occurring at conventional AF/F interfaces, the exchange coupling between the AF and F superlattices in our double superlattice structures is less sensitive to roughness and can be considered uniform across the interface. The double superlattice structure is different from the spin valves where a synthetic antiferromagnet replaces the pinned layer,²¹ because in those spin valves the sensing layer is not coupled to the synthetic antiferromagnet.

Of present interest are double superlattice structures with the AF superlattice having a configuration $[\text{Fe}(14 \text{ \AA})/\text{Cr}(11 \text{ \AA})]_{20}$, while the F superlattice is $[\text{Fe}(50 \text{ \AA})/\text{Cr}(20 \text{ \AA})]_{n_F}$ with $n_F=2, 3, 5,$ and 10 . The numbers inside the parentheses denote the layer thicknesses, and the subscripts denote the number of repetitions of the Fe/Cr bilayer unit. The Cr layer between the AF and F superlattices is 20-Å thick and gives rise to ferromagnetic intersuperlattice coupling. The Fe/Cr double superlattices were grown via dc magnetron sputtering onto single-crystal MgO(110) substrates. A 200-Å Cr buffer layer was first deposited at 400 °C to establish epitaxy with the substrate. The double superlattice structure was then grown at 100 °C, followed by a 50-Å Cr cover layer. Samples with only a single AF or F Fe/Cr superlattice were also prepared similarly for benchmarking. The structures were characterized by x-ray diffraction using Cu $K\alpha$ radiation. The crystal structure is bcc. For the single Fe/Cr superlattices, high-angle superlattice diffraction peaks up to third order were observed. Asymmetric azimuthal scans confirmed the expected in-plane epitaxial relations: $\text{Fe/Cr}[0\bar{1}1]\|\text{MgO}[001]$ and $\text{Fe/Cr}[\bar{1}11]\|\text{MgO}[1\bar{1}0]$. The anisotropy constant determined from the hard-axis magnetization curves agrees with the published value $K_S = 0.06 \text{ erg/cm}^2$.²⁰ The anisotropy fields are 1.6 kOe for 14-Å Fe layers, and 450 Oe for 50-Å Fe layers.

Shown in Fig. 1 is the room-temperature magnetization curve of a double superlattice with $n_F=5$ measured by superconducting quantum interference device (SQUID) magnetometry along the easy direction. The magnetization is normalized with respect to the full saturation value. Since the Fe moment in the F superlattice comprises 47% of the total moment, the transition between +0.47 and -0.47 in the normalized magnetization in low field represents the F superlat-

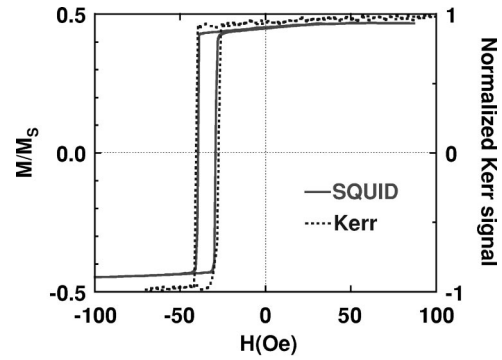


FIG. 2. Minor hysteresis loops of the Fe/Cr double superlattice of Fig. 1 after alignment at +20 kOe. The solid line is measured by SQUID magnetometry and the dashed line by means of the magneto-optic Kerr effect. The magnetization is normalized to the full saturation value.

tice, while the AF superlattice contributes zero net magnetization. The kinks in magnetization marked by arrows identify the spin-flop transitions in the AF superlattice.²² With increasing field, the Fe moments in the AF rotate from a spin-flopped state toward parallel alignment and the magnetization gradually increases. The field values for the spin-flop transition (2 kOe) and for saturation (14 kOe) are identical to those of the AF superlattices in Ref. 20 with the same layer thicknesses.

In a conventional AF/F exchange-bias system, cooling in a field through the Néel temperature of the AF is required to establish a unidirectional magnetic anisotropy. However, this is not necessary for our AF/F double superlattice structures. Figure 2 shows a minor hysteresis loop of the same double superlattice measured in fields between ± 200 Oe, after a large field of +20 kOe had been applied to align all Fe layers in both F and AF superlattices. The minor loop is displaced from zero in the negative field direction by 34.4 Oe.²³ The shifted hysteresis loop is indicative of the unidirectional anisotropy. The aligning field breaks the symmetry and leaves the interfacial Fe layer of the AF superlattice necessarily parallel to the alignment direction. The exchange interaction between the F superlattice and the interfacial Fe layer then causes the hysteresis loop of the F superlattice to shift toward the negative direction. Note that the width of the hysteresis loops is only ~ 10 Oe, which is much smaller than the anisotropy field. This indicates that the magnetization reversal of the F superlattice is not by coherent rotation, but rather by nucleation and growth of reverse magnetic domains. Also shown in Fig. 2 is the minor loop measured using the magneto-optic Kerr effect. Since the Kerr effect is sensitive to the magnetization on the scale of the optical penetration depth ($\sim 200 \text{ \AA}$), which is roughly the thickness of the F superlattice, the single-stepped switching in Kerr intensity indicates that all of the Fe layers, the F superlattice, reverse their magnetization simultaneously. The sharpness of the switching indicates pinning-free domain wall motion. Therefore, the exchange coupling manifests itself as a bias field at the onset of domain reversal. It is worth noting that the models of Refs. 11, 12, and 13 imply a coherent rotation of the F magnetization, and that the scenario of nucleation and growth of reverse domains in exchange-bias systems is discussed only indirectly in Ref. 15.

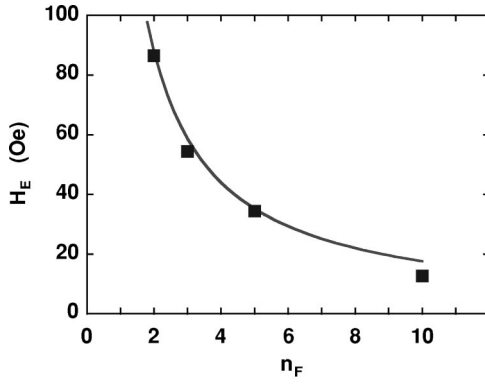


FIG. 3. The exchange-bias field H_E as a function of the number of Fe layers in the F superlattice, n_F . The solid curve is the calculated exchange-bias field as described in the text.

In Fig. 3, the values of the exchange-bias field H_E for several double superlattices are shown as a function of n_F , the number of Fe layers in the F superlattices. With increasing n_F , H_E decreases monotonically. The classic formula for the magnitude of the exchange-bias field as applied to systems of collinear spin structures is

$$H_E = J_{int} / t_F M_F, \quad (1)$$

where J_{int} is the interfacial exchange-coupling energy, and t_F and M_F are the thickness and magnetization of the ferromagnet, respectively. In the present $[\text{Fe}/\text{Cr}]^{AF}/\text{Cr}/[\text{Fe}/\text{Cr}]^F$ double superlattices, the equivalent interfacial exchange interaction is the coupling across the center Cr layer, and $t_F M_F = n_F d_{\text{Fe}}^F M_{\text{Fe}}$, where d_{Fe}^F is the Fe layer thickness in the F superlattice, and M_{Fe} is the saturation magnetization of Fe. Using the previously determined interlayer coupling energy across a 20-Å Cr spacer layer $J_F = 0.07$ erg/cm² (Ref. 20), ($J_{int} = 2J_F$, since J_F was defined as the coupling strength per Fe layer in a bilayer structure²⁴), $d_{\text{Fe}}^F = 50$ Å, and $M_{\text{Fe}} = 1700$ emu/cm³, we have calculated the expected exchange-bias field from Eq. (1) and plotted it as the solid curve in Fig. 3. Such a comparison is possible only because

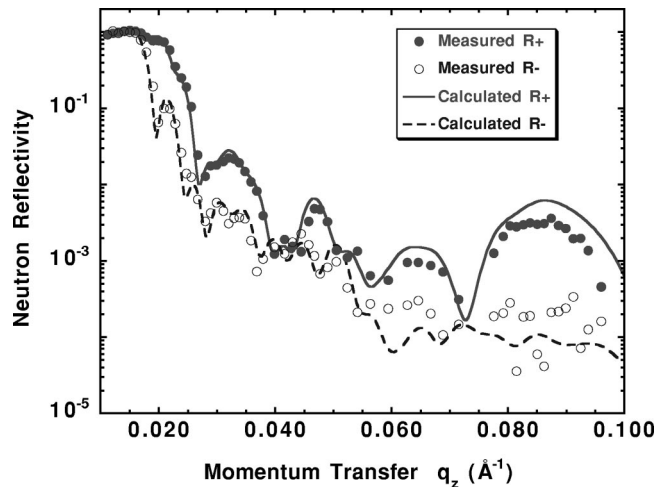


FIG. 4. Measured and calculated polarized neutron reflectivity for the double superlattice of Fig. 1 in a field $H = -35$ Oe for neutrons with spin parallel to H (full points/full line) and antiparallel to H (open points/dashed line).

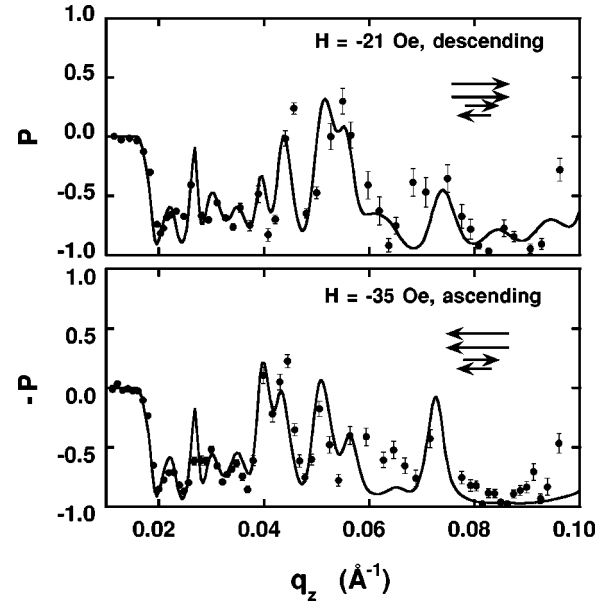


FIG. 5. Top: Spin asymmetry P for the double superlattice of Fig. 1 in a descending field of $H = -21$ Oe. Bottom: $-P$ for the same sample in an ascending field $H = -35$ Oe. The curves are calculations assuming a collinear spin profile. The diagrams illustrate the spin configurations near the AF/ F interface. The parallel arrows indicate the magnetization directions of the Fe layers in the F superlattice and the antiparallel arrows indicate those in the AF superlattice.

the highly ideal AF/ F interfaces in double superlattices permit unambiguous determination of J_{int} . Note that whereas the classic formula overestimates the exchange-bias field by two orders of magnitude in conventional AF/ F systems, the data points in Fig. 3 are well described by Eq. (1) with the exact value for J_{int} . However, since exchange biasing occurs at the onset of domain reversal, the quantitative agreement between measured and calculated exchange-bias fields in the double superlattices advocates that the region of significance for exchange bias includes only the volume of the nucleated reverse domain in the F and the part of the AF that is exchange coupled to it, rather than the entire volume of the AF/ F system.

Polarized neutron reflectivity (PNR) measurements were taken in order to determine the layer-by-layer magnetization of the double superlattice, both in size and orientation.²⁵ The momentum transfer of the neutron perpendicular to the surface $q_z = 4\pi \sin \theta / \lambda$, where θ is the angle of the neutron beam with respect to the surface plane, and λ is the neutron wavelength. As a rule of thumb the spatial resolution is the inverse of the maximum value of q_z that has been measured. The PNR measurements were taken at the ‘‘POSY I’’ instrument at Argonne’s Pulsed Neutron source. The sample had $n_F = 5$ ferromagnetic layers and a surface area of 6×6 mm². Two scans were taken at room temperature in the two branches of a minor loop after aligning the sample in a field of +20 kOe. They were, respectively, in a field of -21 Oe, with the ferromagnet magnetized in the direction of the aligning field; and -35 Oe after cycling to -120 Oe, where the ferromagnet is magnetized in the opposite direction. Figure 4 shows the reflectivities for neutrons polarized parallel (R_+) and antiparallel (R_-) to the applied

magnetic field $H = -35$ Oe. It is interesting to describe the physical significance of the main features of the spectra. The strong spin dependence of the reflectivity indicates the presence of large magnetic induction fields in the sample, parallel to the applied field. At the left side of Fig. 4, the critical angle is characteristic of the MgO substrate, while at the right side, the broad ferromagnetic peak appears (the first AF peak is out of the q_z range presented here). The most pronounced interference fringes of the + polarized neutrons correspond to the total thickness of the F superlattice. Also indicated in Fig. 4 is the reflectivity calculated assuming a *collinear* distribution of the spins of the F and the AF components—with the magnetization of the first AF layer opposite to that of the F superlattice. The spin asymmetry $P = (R_+ - R_-)/(R_+ + R_-)$ is shown in Fig. 5 for the two magnetization branches. The measurements show a pronounced difference at $q_z = 0.05$. This is the region where the calculated asymmetries are most sensitive to the reversal of the magnetization in the F superlattice. Since noncollinear configurations do not contribute to the asymmetry (the rel-

evant magnetic and nuclear amplitudes are in quadrature), this result provides the most direct confirmation hitherto obtained of a collinear spin configuration in an exchange-bias system.

In conclusion, we have demonstrated exchange-bias behavior in double-superlattice structures that utilizes oscillatory interlayer exchange coupling. The exchange-bias field agrees quantitatively with the classical formula and polarized neutron reflectivity measurements confirm the collinear spin distribution. While there is no straightforward way to characterize and manipulate the interfacial coupling in conventional exchange-bias systems, our double superlattice structures have highly ideal AF/F interfaces. The flexibility in configuration, and tunable coupling strength and magnetic anisotropy offered by the double superlattice structures should create new opportunities to elucidate the underlying physics of the exchange-bias phenomenon.

This work was supported by U.S. DOE, BES-MS, Contract No. 31-109-ENG-38.

-
- ¹J. Nogués and I. K. Schuller, *J. Magn. Magn. Mater.* **192**, 203 (1999), and references therein.
- ²W. H. Meiklejohn and C. P. Bean, *Phys. Rev.* **105**, 904 (1957).
- ³J. S. Kouvel, *J. Phys. Chem. Solids* **16**, 132 (1960).
- ⁴A. E. Berkowitz and J. H. Greiner, *J. Appl. Phys.* **36**, 3330 (1965).
- ⁵R. Jungblut, R. Coehoorn, M. T. Johnson, Ch. Sauer, P. J. van der Zaag, A. R. Ball, Th. G. S. M. Rijks, J. aan de Stegge, and A. Reinders, *J. Magn. Magn. Mater.* **148**, 300 (1995).
- ⁶T. J. Moran, J. M. Gallego, and I. K. Schuller, *J. Appl. Phys.* **78**, 1887 (1995).
- ⁷J. Nogués, D. Lederman, T. J. Moran, I. K. Schuller, and K. V. Rao, *Appl. Phys. Lett.* **68**, 3186 (1996).
- ⁸N. J. Gökemeijer, T. Ambrose, and C. L. Chien, *Phys. Rev. Lett.* **79**, 4270 (1997).
- ⁹C. Tang, *J. Appl. Phys.* **55**, 2226 (1984); B. Dieny, V. S. Sперiosu, S. S. P. Parkin, D. R. Wilhoit, and D. Mauri, *Phys. Rev. B* **43**, 1297 (1991).
- ¹⁰W. H. Meiklejohn, *J. Appl. Phys.* **33**, 1328 (1962).
- ¹¹D. Mauri, H. C. Siegmann, P. S. Bagus, and E. Kay, *J. Appl. Phys.* **62**, 3047 (1987).
- ¹²A. P. Malozemoff, *Phys. Rev. B* **35**, 3679 (1987).
- ¹³N. C. Koon, *Phys. Rev. Lett.* **78**, 4865 (1997).
- ¹⁴T. J. Moran, J. Nogués, D. Lederman, and I. K. Schuller, *Appl. Phys. Lett.* **72**, 617 (1998).
- ¹⁵T. C. Schulthess and W. H. Butler, *Phys. Rev. Lett.* **81**, 4516 (1998).
- ¹⁶K. Takano, R. H. Kodama, A. E. Berkowitz, W. Cao, and G. Thomas, *Phys. Rev. Lett.* **79**, 1130 (1997).
- ¹⁷S. S. P. Parkin, V. R. Deline, R. O. Hilleke, and G. P. Felcher, *Phys. Rev. B* **42**, 10 583 (1990); G. P. Felcher, Y. Y. Huang, M. Carey, and A. E. Berkowitz, *J. Magn. Magn. Mater.* **121**, 105 (1993).
- ¹⁸S. S. P. Parkin and D. Mauri, *Phys. Rev. B* **44**, 7131 (1991).
- ¹⁹S. S. Parkin, N. More, and K. P. Roche, *Phys. Rev. Lett.* **64**, 2304 (1990); J. Unguris, R. J. Celotta, and D. T. Pierce, *ibid.* **67**, 140 (1991).
- ²⁰E. E. Fullerton, M. J. Conover, J. E. Mattson, C. H. Sowers, and S. D. Bader, *Phys. Rev. B* **48**, 15 755 (1993); *J. Appl. Phys.* **75**, 6461 (1994).
- ²¹V. Sперiosu, B. A. Gurney, D. R. Wilhoit, and L. B. Brown (unpublished).
- ²²R. W. Wang, D. L. Mills, E. E. Fullerton, J. E. Mattson, and S. D. Bader, *Phys. Rev. Lett.* **72**, 920 (1994).
- ²³To correct for the remanent field due to trapped flux in the superconducting magnet of the SQUID magnetometer, a second minor loop was measured with the sample rotated by 180°. The midpoint between the centers of the two minor loops defines the zero-field point.
- ²⁴W. Folkerts, *J. Magn. Magn. Mater.* **94**, 302 (1991).
- ²⁵H. Zabel, *Physica B* **198**, 156 (1994).